Reduced uncertainty of the axial γZ-box diagram correction to the proton's weak charge

Jens Erler,[1,2] Mikhail Gorchtein,[3] Oleksandr Koshchii,[1] Chien-Yeah Seng,[4,*] and Hubert Spiesberger[1,5]

[1]*PRISMA$^+$ Cluster of Excellence, Institut für Physik, Johannes Gutenberg-Universität, Mainz D-55099, Germany*

[2]*Departamento de Física Teórica, Instituto de Física, Universidad Nacional Autónoma de México, 04510 CDMX, México*

[3]*PRISMA$^+$ Cluster of Excellence, Institut für Kernphysik, Johannes Gutenberg-Universität, Mainz D-55099, Germany*

[4]*Helmholtz-Institut für Strahlen- und Kernphysik and Bethe Center for Theoretical Physics, Universität Bonn, 53115 Bonn, Germany*

[5]*Centre for Theoretical and Mathematical Physics and Department of Physics, University of Cape Town, Rondebosch 7700, South Africa*

(Received 24 July 2019; published 17 September 2019)

We present the fully up-to-date calculation of the γZ-box correction which needs to be taken into account to determine the weak mixing angle at low energies from parity-violating electron proton scattering. We make use of neutrino and antineutrino inclusive scattering data to predict the parity-violating structure function $F_3^{\gamma Z}$ by isospin symmetry. Our new analysis confirms previous results for the axial contribution to the γZ-box graph and reduces the uncertainty by a factor of 2. In addition, we note that the presence of parity-violating photon-hadron interactions induces an additional contribution via $F_3^{\gamma\gamma}$. Using experimental and theoretical constraints on the nucleon anapole moment we are able to estimate the uncertainty associated with this contribution. We point out that future measurements are expected to significantly reduce this latter uncertainty.

DOI: 10.1103/PhysRevD.100.053007

I. INTRODUCTION

The precision measurement of $s_W^2 \equiv \sin^2\theta_W$, where θ_W is the Standard Model (SM) weak mixing angle, in parity-violating (PV) electron scattering serves as a powerful tool to test the SM and search for physics beyond it. Since the energy dependence of s_W^2 is very precisely predicted within the SM [1], any significant deviation from it would be an indication of beyond Standard Model (BSM) physics. Polarized elastic ep scattering in the limit of vanishing beam energy E and momentum transfer t probes the so-called weak charge of the proton:

$$Q_W^p = -\lim_{|t|\to 0}\frac{4\sqrt{2}\pi\alpha}{G_F|t|}\frac{d\sigma_+ - d\sigma_-}{d\sigma_+ + d\sigma_-}\bigg|_{E=0}. \tag{1}$$

Here, α is the fine structure constant and G_F the Fermi constant. $d\sigma_\pm$ are the differential cross sections for scattering with right-handed and left-handed polarized electrons, respectively. At tree level this quantity is given by $1-4s_W^2$, which is accidentally suppressed. This effectively leads to an enhancement in the sensitivity to s_W^2,

$$\frac{\Delta s_W^2}{s_W^2} \approx 0.08\,\frac{\Delta Q_W^p}{Q_W^p}, \tag{2}$$

which also implies an enhanced sensitivity to BSM effects that may enter the running of s_W^2. As a concrete example, the upcoming P2 experiment at the Mainz Energy-Recovering Superconducting Accelerator (MESA), that plans for a measurement of the proton weak charge to 1.4% with a beam energy of $E = 155$ MeV, will lead to a determination of s_W^2 to 0.15% precision [2].

Due to its accidental suppression at tree level, one needs to carefully account for all the SM higher-order effects to Q_W^p in order to properly translate the high-precision experimental measurements into a determination of the weak mixing angle and constraints on BSM parameters. Including one-loop electroweak radiative corrections, the proton weak charge reads [3]

*Corresponding author.
cseng@hiskp.uni-bonn.de

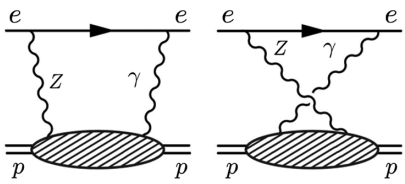

FIG. 1. The γZ box diagrams. Not shown are the two remaining diagrams with γ and Z interchanged.

$$Q_W^p = (1+\Delta\rho+\Delta_e)(1-4s_W^2(0)+\Delta_e') + \Box_{WW} + \Box_{ZZ} + \Box_{\gamma Z}(0). \tag{3}$$

Among them, the quantity $\Box_{\gamma Z}$ which denotes the contribution from the γZ box diagram (see Fig. 1) contains sensitivity to physics at the hadronic scale where perturbative calculations are unreliable, inducing a large theoretical uncertainty. It is in general a function of E and can be split into two terms:

$$\Box_{\gamma Z}(E) = \Box_{\gamma Z}^V(E) + \Box_{\gamma Z}^A(E), \tag{4}$$

where the superscript $V(A)$ denotes the contribution from the vector (axial-vector) weak neutral current on the hadron side. The axial box is nonzero at $E=0$ but suppressed by the small electron weak vector coupling $v_e = -(1-4s_W^2)$. On the other hand, the vector box is not suppressed by any small coefficient but is exactly zero at $E=0$.

Earlier studies of $\Box_{\gamma Z}$ [4–6] assume small E and hence are sensitive only to the axial box. However, a reanalysis in 2009 based on a dispersion relation [7] revealed a steep energy dependence in $\Box_{\gamma Z}^V(E)$ which was not previously accounted for. This finding stimulated a large number of follow-up studies on the vector γZ box [8–14] as the latter was found to play a dominant role in the extraction of the proton weak charge in the Qweak experiment which took data at $E = 1.165$ GeV [15]. These studies consistently concluded that the theoretical uncertainty in $\Box_{\gamma Z}^V(E)$ increases with E, which also motivated future measurements of Q_W^p (specifically, the P2 experiment) to be performed with lower beam energy.

Unlike its vector counterpart, there are much fewer follow-up theoretical studies of $\Box_{\gamma Z}^A(E)$ [12,16–18], despite its becoming increasingly important at small E. In particular, no attempt was made so far to relate the contributions from multihadron intermediate states at small momentum transfers below about 1 GeV^2 to experimental data, and all existing studies of these contributions are based on *ad hoc* models where a systematic uncertainty analysis is difficult or impossible.

In this paper we present an updated study of the axial γZ box by adopting a Regge parameterization of the multihadron contributions with parameters fitted to inclusive $\nu p/\bar{\nu}p$ scattering data. This technique was recently introduced in the treatment of the axial γW box diagram in neutron and nuclear β decay [19,20]. We will show that by employing the neutrino data one is able to further reduce the uncertainty in $\Box_{\gamma Z}^A$ quoted in Ref. [16] by a factor of 2. Within the same theoretical framework, we further discuss a contribution which arises from the parity-odd component in the $\gamma\gamma$ box. It possesses the same theoretical structure as $\Box_{\gamma Z}^A$ and is therefore inseparable from the latter. Using the current constraints on the nucleon anapole moment, we provide an estimate on the additional theory uncertainty induced by this term.

II. DISPERSIVE REPRESENTATION OF $\Box_{\gamma Z}^A$

We start from the dispersive representation of $\Box_{\gamma Z}^A$ derived in Ref. [16] for the case of electron scattering in the forward direction:

$$\Box_{\gamma Z}^A(E) = \frac{2}{\pi}\int_0^\infty dQ^2 \frac{v_e(Q^2)\alpha(Q^2)}{Q^2(1+Q^2/M_Z^2)} \times \int_0^1 dx F_3^{\gamma Z}(x,Q^2) f(r,t'), \tag{5}$$

where

$$f(r,t') = \frac{1}{t'^2}\mathrm{Re}\left[\ln\left(1-\frac{t'^2}{r^2}\right) + 2t'\tanh^{-1}\left(\frac{t'}{r}\right)\right] \tag{6}$$

with $x = Q^2/(W^2-M^2+Q^2)$, $r = 1+\sqrt{1+4M^2x^2/Q^2}$, $t' = 4MEx/Q^2$, and M the nucleon mass. We will take into account that in the $\overline{\mathrm{MS}}$ scheme both s_W^2 and α are running, i.e., scale-dependent parameters. We calculate them as described in Refs. [1,21], respectively. The spin-independent, parity-odd structure function $F_3^{\gamma Z}$ is defined through the hadronic tensor

$$\frac{1}{4\pi}\int d^4x e^{iq\cdot x}\langle p(p)|[J_{em}^\mu(x),(J_Z^\nu(0))_A]|p(p)\rangle = -\frac{i\varepsilon^{\mu\nu\alpha\beta}q_\alpha p_\beta}{2p\cdot q}F_3^{\gamma Z}(x,Q^2), \tag{7}$$

where p is the 4-momentum of the incoming proton, q the 4-momentum transfer with $q^2=-Q^2$, and $\varepsilon^{0123}=-1$. The electromagnetic and weak neutral currents read

$$J_{em}^\mu = \sum_q e_q\bar{q}\gamma^\mu q, \qquad J_Z^\mu = (J_Z^\mu)_V + (J_Z^\mu)_A,$$
$$(J_Z^\mu)_V = \sum_q g_V^q\bar{q}\gamma^\mu q, \qquad (J_Z^\mu)_A = \sum_q g_A^q\bar{q}\gamma^\mu\gamma_5 q, \tag{8}$$

with $e_u = 2/3$, $e_d = e_s = -1/3$, $g_V^q = 2(I_{3,L}^q - 2e_q s_W^2)$, and $g_A^q = -2I_{3,L}^q$. In particular, when $E=0$ one finds the simplification [20]

$$\Box^A_{\gamma Z}(0)=\frac{3}{2\pi}\int_0^\infty \frac{dQ^2}{Q^2}\frac{v_e(Q^2)\alpha(Q^2)}{1+Q^2/M_Z^2}M_3^{\gamma Z}(1,Q^2), \quad (9)$$

where

$$M_3^{\gamma Z}(1,Q^2)=\frac{4}{3}\int_0^1 dx\frac{2r-1}{r^2}F_3^{\gamma Z}(x,Q^2) \quad (10)$$

is the first Nachtmann moment of $F_3^{\gamma Z}$ [22,23].

It is important to identify the dominant contributions to the structure function $F_3^{\gamma Z}$ at different Q^2 and $W^2=(p+q)^2$, as we summarize in Fig. 2. One can write

$$F_3^{\gamma Z}=F_{3,\mathrm{el}}^{\gamma Z}+F_{3,\mathrm{inel}}^{\gamma Z}, \quad (11)$$

separating the elastic (sometimes called Born) contribution that represents an isolated peak at $W^2=M^2$ and all the inelastic contributions that start to emerge above the single-pion production threshold $W^2=(M+m_\pi)^2$. The latter can be further subdivided in Q^2:

$$F_{3,\mathrm{inel}}^{\gamma Z}=\begin{cases} F_{3,\pi N}^{\gamma Z}+F_{3,\mathrm{res}}^{\gamma Z}+F_{3,\mathbb{R}}^{\gamma Z} & (Q^2<2\ \mathrm{GeV}^2) \\ F_{3,\mathrm{DIS}}^{\gamma Z} & (Q^2>2\ \mathrm{GeV}^2). \end{cases} \quad (12)$$

First, above $Q^2\simeq 2\ \mathrm{GeV}^2$, in the deep-inelastic scattering (DIS) regime, the structure functions are well described by the parton model including corrections from perturbative quantum chromodynamics (pQCD). This is corroborated by the observation that the pQCD-corrected Gross–Llewellyn-Smith (GLS) sum rule [24] is well satisfied at $Q^2>2\ \mathrm{GeV}^2$ in $\nu p/\bar{\nu}p$ scattering experiments [25,26].

In contrast, at lower Q^2 the effective degrees of freedom are hadrons. It was pointed out recently that nonperturbative contributions can in principle be obtained from lattice QCD [27], but before such calculations are carried out and the respective uncertainties are well understood, we have to rely on a model constrained by the experimental input.

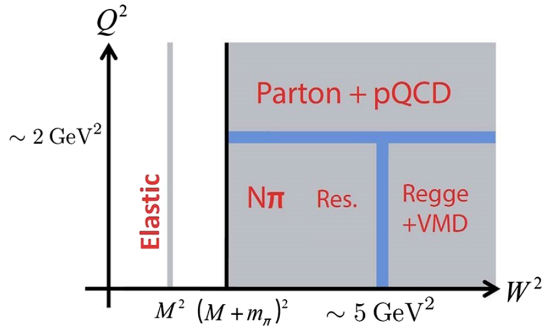

FIG. 2. Dominant physics that enter $F_3^{\gamma Z}$ in different regions in the W^2-Q^2 plane.

The lowest inelastic hadronic state, the $N\pi$ continuum, starts contributing above its production threshold. In the range $1.5\ \mathrm{GeV}^2<W^2<5\ \mathrm{GeV}^2$ one observes nucleon resonances. Above the two-pion threshold at $(M+2m_\pi)^2$ multihadron states emerge which become dominant at large W^2. The Regge exchange picture provides an economical description of these contributions which we smoothly continue down to the two-pion threshold, as described in the following. We furthermore use the vector meson dominance (VMD) picture to extend the Regge description to moderate values of Q^2. We label this contribution by the subscript "$\mathbb{R}$." Correspondingly, we obtain the γZ-box correction as a sum of five contributions:

$$\Box^A_{\gamma Z}(E)=\sum_i \Box^{A,i}_{\gamma Z}(E), \quad (13)$$

with $i=\mathrm{el}$, πN, res, $\mathbb{R}$, and DIS. Each contribution is computed by inserting the corresponding $F_{3,i}^{\gamma Z}$ into Eq. (5) and integrating over its support in W and Q^2.

The elastic contribution is given in terms of the proton magnetic Sachs form factor G_M^p and the axial form factor G_A:

$$F_{3,\mathrm{el}}^{\gamma Z}(x,Q^2)=-G_M^p(Q^2)G_A(Q^2)\delta(1-x). \quad (14)$$

In the numerical evaluation of this part we adopt recent data on these form factors as given in Refs. [28,29].

The DIS region contribution to the box diagram can be represented as an infinite sum of odd Mellin moments of $F_3^{\gamma Z}$ upon expanding the function $f(r,t')$ in Eqs. (5) and (6) in powers of x^2M^2/Q^2 [16]. None of the even Mellin moments of $F_3^{\gamma Z}$ appear due to the symmetry of the integrands in x. The result is almost E independent. Furthermore, the size of contributions from the third and higher moments to $\Box^A_{\gamma Z}$ is about 10^{-5}. It is 2 orders of magnitude below that from the first Mellin moment and has little impact on the final result. The first Mellin moment is independent of the details of the parton distribution functions and its pQCD correction has previously been considered up to $\mathcal{O}(\alpha_s)$. For completeness, we include here the full $\mathcal{O}(\alpha_s^4)$ expression [30,31]:

$$\int_0^1 dx F_{3,\mathrm{DIS}}^{\gamma Z}(x,Q^2) = \frac{5}{3}\left[1-\frac{\alpha_s}{\pi}-c_2\frac{\alpha_s^2}{\pi^2}-c_3\frac{\alpha_s^3}{\pi^3}-c_4\frac{\alpha_s^4}{\pi^4}\right]-\frac{3}{2}\frac{\alpha_s^3}{\pi^3}\left[s_3+s_4\frac{\alpha_s}{\pi}\right]. \quad (15)$$

The first term on the right-hand side [30] represents the isosinglet piece satisfying the polarized Bjorken sum rule [32]. It receives only contributions from nonsinglet (connected) diagrams. The second term [31] contributes only to

the isotriplet piece by singlet (disconnected) diagrams and enters the GLS [24] sum rule. The coefficients in numerical form are given by [30,31]

$$\begin{aligned} c_2 &= 4.583 - 0.333 n_f, \\ c_3 &= 41.44 - 7.607 n_f + 0.177 n_f^2, \\ c_4 &= 479.4 - 123.4 n_f + 7.697 n_f^2 - 0.1037 n_f^3, \\ s_3 &= -0.413 n_f, \\ s_4 &= -5.802 n_f + 0.2332 n_f^2. \end{aligned} \tag{16}$$

In the numerical evaluation, we use the running strong coupling constant α_s provided by the *Mathematica* code RunDec [33] with $\alpha_s(M_Z) = 0.118$, and values for the number of flavors, n_f, changing by one unit at quark mass thresholds as implemented in RunDec. Integrating this expression with $Q^2_{\rm min} = 2\ {\rm GeV}^2$ in Eq. (5) results in a contribution of 30.4×10^{-4} to $\Box^A_{\gamma Z}$. We note that our $\mathcal{O}(\alpha_s^4)$ result differs from the $\mathcal{O}(\alpha_s)$ result by only about 2%. We have also checked that using $Q^2_{\rm min} = 1\ {\rm GeV}^2$ and the $\mathcal{O}(\alpha_s)$ expression we obtain 32.9×10^{-4} in good agreement with Ref. [16].

Higher twist (HT) effects represent a source of the possible uncertainty in the lower Q^2 part of the DIS region, $2\ {\rm GeV}^2 < Q^2 < 5\ {\rm GeV}^2$. Since we have experimental data to compare with the pQCD prediction, we assume that the uncertainty due to HT contributions should not exceed that of the data, which is ∼5%. This uncertainty would be a systematical one, and we will use as the estimate 5% of the integral of the DIS contribution over this Q^2 range. Numerically, it amounts to 1.3×10^{-5}, which we include in the total error.

The $N\pi$ contribution is calculated within the framework of chiral perturbation theory but with pointlike electroweak vertex couplings replaced by the Dirac and axial nucleon form factors, which suppresses their high-Q^2 contribution. Details of this calculation are described in Ref. [20]. We assign a generous 30% uncertainty due to higher chiral orders. This uncertainty, however, does not affect the total error budget.

As for the resonances, our treatment is the same as in Ref. [16]. The only numerically relevant contribution is due to the Δ resonance, which we calculate using the parameterization in Ref. [34]. As there are no assigned uncertainties for the values of the parameters, it is not possible to provide an error estimate for the Δ contribution to $\Box^A_{\gamma Z}$. This contribution is small, at the level of the overall uncertainty, and even a conservative 30% uncertainty hardly modifies the total error. Moreover, we note here that the resonance and multihadron contributions are anticorrelated, as it is their sum that is constrained by measured experimental cross sections. A significant increase in one will have to be compensated for by a reduction in the other, so that the overall effect is smaller than if this anticorrelation was naïvely neglected. We therefore opt to exclude the resonance uncertainty from the total error.

The treatment of multihadron intermediate states requires more care. Following Refs. [19,20], we establish the correspondence between $F_3^{\gamma Z}$ and its charged current counterpart $F_3^{\nu p+\bar\nu p}$ by isospin symmetry. The electromagnetic current can be decomposed into isosinglet and isotriplet components:

$$J^\mu_{\rm em} = J^{\mu(0)}_{\rm em} + J^{\mu(1)}_{\rm em}. \tag{17}$$

Likewise, we can also separate the structure function $F_3^{\gamma Z}$ into isosinglet and isotriplet parts, $F_3^{\gamma Z} = F_{3(0)}^{\gamma Z} + F_{3(1)}^{\gamma Z}$, where the axial part of the Z current is purely isovector. Upon neglecting strange quarks, we find through an isospin rotation that the $(I=1) \otimes (I=1)$ isospin channel $F_{3(1)}^{\gamma Z}$ equals half of the structure function $F_3^{\nu p+\bar\nu p}$ that accounts for the difference of the cross sections for inclusive νp and $\bar\nu p$ scattering [35]. We thus obtain the model-independent expression

$$F_3^{\gamma Z} = \frac{1}{2} F_3^{\nu p+\bar\nu p} + F_{3(0)}^{\gamma Z}. \tag{18}$$

There are two advantages in doing so, as (a) data exist for $F_3^{\nu p+\bar\nu p}$ at moderate Q^2 where a first-principle theory description is not available, and (b) $J^\mu_{\rm em}$ is predominantly isovector, so that the contribution from $F_{3(0)}^{\gamma Z}$ is small. Therefore, utilizing neutrino data, one obtains a model-independent determination of the dominant isotriplet piece, limiting the model dependence to the small isosinglet piece. Apart from the use of isospin symmetry, our treatment differs from that in Ref. [16] in that we account for continuous backgrounds already starting at the two-pion threshold $W^2 = (M + 2m_\pi)^2$.

Our parameterization is based on the leading Regge trajectory exchange picture introduced in Refs. [19,20], where the reader can find more details. The respective diagrams are shown in Fig. 3. In this picture and making use of the nearly exact degeneracy between the ω and ρ mesons, the isosinglet and isovector pieces are related to each other and to their charged current counterpart in a simple way:

$$F^{\gamma Z}_{3,\mathbb{R}(0)} = \frac{f_{\rm th}}{18} C_{WW} \frac{m_\omega^2}{m_\omega^2 + Q^2} \frac{m_{a_1}^2}{m_{a_1}^2 + Q^2} \left(\frac{\nu}{\nu_0}\right)^{\alpha_0}, \tag{19}$$

$$\begin{aligned} F^{\gamma Z}_{3,\mathbb{R}(1)} &= \frac{f_{\rm th}}{2} C_{WW} \frac{m_\rho^2}{m_\rho^2 + Q^2} \frac{m_{a_1}^2}{m_{a_1}^2 + Q^2} \left(\frac{\nu}{\nu_0}\right)^{\alpha_0} \\ &= \frac{1}{2} F^{\nu p+\bar\nu p}_{3,\mathbb{R}}, \end{aligned} \tag{20}$$

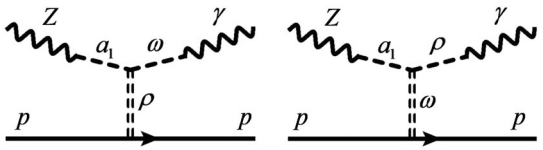

FIG. 3. Regge exchange diagrams giving rise to the isosinglet, $F^{\gamma Z}_{3,\mathbb{R}(0)}$, and isotriplet, $F^{\gamma Z}_{3,\mathbb{R}(1)}$, parts of $F^{\gamma Z}_{3,\mathbb{R}}$, respectively.

with $\alpha_0 \approx 0.477$ the intercept of the ω/ρ trajectory, $\nu = Q^2/2Mx$, and $\nu_0 = 1$ GeV a typical hadronic scale. The threshold function that suppresses the small-W^2 contribution was chosen in the form

$$f_{\rm th} = \Theta(W^2 - W_{\rm th}^2)(1 - e^{(W_{\rm th}^2 - W^2)/\Lambda_{\rm th}^2}), \qquad (21)$$

where $\Lambda_{\rm th} = 1$ GeV and $W_{\rm th}^2 = (M + 2m_\pi)^2$ is the two-pion threshold. As in Ref. [19], we assume that it is sufficient to take $C_{WW} = C_{WW}(Q^2)$ as linear, $C_{WW} = A_{WW}(1 + B_{WW}Q^2)$. The parameter values $A_{WW} = 5.2 \pm 1.5$ and $B_{WW} = 1.08^{+0.48}_{-0.28}$ GeV^{-2} [19] have been obtained from a fit of the first Nachtmann moment of $F_3^{\nu p + \bar{\nu} p}$ using data from CCFR [25,26], BEBC/Gargamelle [36] and WA25 [37], after subtracting the elastic, $N\pi$, and resonance pieces. Using Eqs. (19) and (20) in Eq. (5) gives the Regge contribution to $\Box^A_{\gamma Z}$.

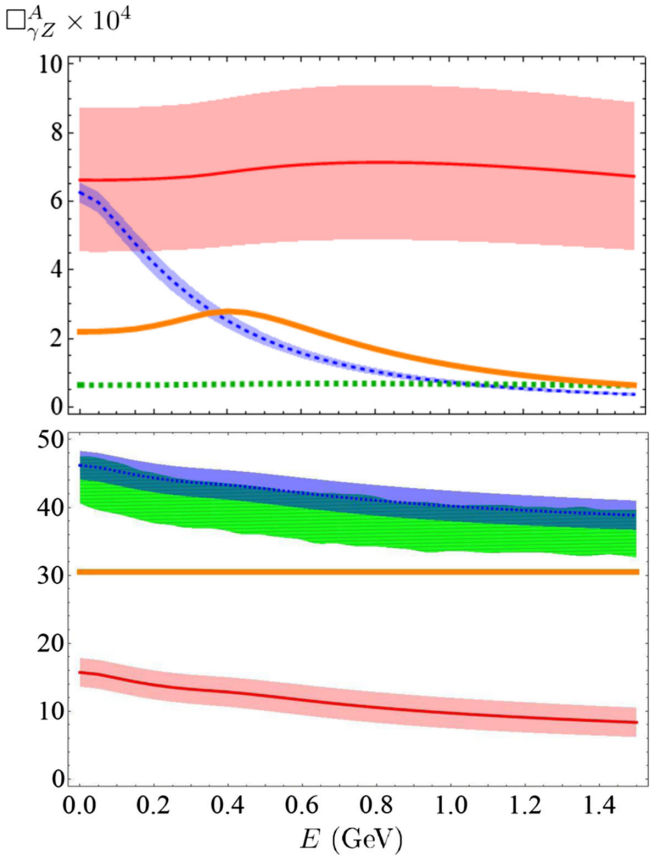

FIG. 4. Upper panel: Summary of all non-DIS contributions to $\Box^A_{\gamma Z}$. Elastic (blue shaded region with dashed central line), resonance (orange solid line), $N\pi$ (green dashed line) and Regge (red shaded region with solid central line) contributions. Lower panel: The DIS contribution (orange line), the sum of all other contributions (red shaded region with solid central line), and the total (blue shaded region with dashed central line). The result of Ref. [16] with its uncertainty band is shown for comparison (green shaded area).

Our results for the $\Box^A_{\gamma Z}$ are shown as function of energy in Fig. 4. The upper panel displays all non-DIS contributions separately, while the lower panel shows their sum, the DIS contribution, and the total, as well as a comparison with the previous evaluation of Ref. [16]. A significant overlap of the uncertainty bands indicates an excellent agreement between the two calculations. In our analysis the uncertainty is reduced by a factor of almost 2.

We visualize the source of this uncertainty reduction in Fig. 5, where we display our Regge contribution to the first Nachtmann moment $M_3^{(1)}(Q^2)/Q^2$ in comparison with the result of the approach of Ref. [16]. That reference assumed no uncertainty beyond $Q^2 = 1$ GeV^2 where the dashed red curve is matched to DIS. Instead, we match the Regge parametrization to DIS at $Q^2 = 2$ GeV^2. The total uncertainty of the $\Box^A_{\gamma Z}$ associated with each approach is obtained by integrating the respective uncertainty band in the displayed range. We see that the use of data to determine the uncertainty of the dispersive calculation allows one to halve the associated theoretical error. The observed close agreement between the solid blue and dashed red curves in the range 1 GeV^2 $< Q^2 <$ 2 GeV^2 demonstrates that there is almost no sensitivity to the exact matching point in this

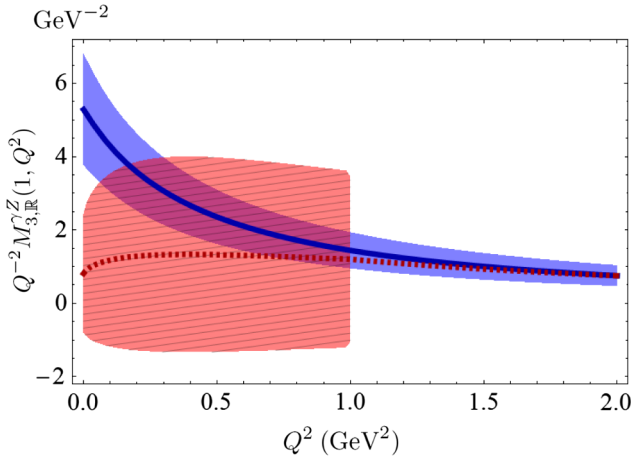

FIG. 5. Our Regge-VMD model result for the first Nachtmann moment of the structure function $F_3^{\gamma Z}$ as a function of Q^2 (solid blue curve for the central value and the shaded area around it for the uncertainty). For comparison, the low-Q^2 DIS contribution of Ref. [16] is shown for $Q^2 < 1$ GeV^2 (dashed red curve for the central value and red shaded area around for the uncertainty).

TABLE I. Individual contributions to $\Box^A_{\gamma Z}(E)$ and associated uncertainties for the P2 and QWeak experiments in units of 10^{-4}. The star at the resonance contribution indicates that it is 100% anticorrelated with the Regge contribution; see the discussion of the uncertainties in the text.

Contribution	$E = 155$ MeV	$E = 1.165$ GeV
Elastic	4.7(3)	0.56(6)
DIS	30.4(1)	30.4(1)
$N\pi$	0.6(2)	0.7(2)
Resonances	2.3(7)*	1.0(3)*
Regge	6.6(2.1)	7.0(2.2)
Total	44.6(2.1)	39.7(2.2)

range, and the respective error is contained in the shaded blue band.

In Table I we list the individual contributions for the kinematics of the two relevant experiments, P2 at MESA with a beam energy of $E = 155$ MeV, and QWeak at JLab with $E = 1.165$ GeV. Our updated analysis provides predictions for the axial γZ box with an uncertainty at the level of 5%. For completeness, we quote here the previous evaluation by Ref. [16]: $\Box^A_{\gamma Z}(E = 0) = 44(4) \times 10^{-4}$ and $\Box^A_{\gamma Z}(E = 1.165\ \text{GeV}) = 37(4) \times 10^{-4}$.

III. PARITY-VIOLATING PHOTON-HADRON INTERACTION

In the previous sections we computed the hadronic structure-dependent one-loop corrections due to the exchange of a γ and a Z boson between the electron and the proton. This calculation requires information on the PV structure function $F_3^{\gamma Z}$ which we obtained by relating it to its charged current partner F_3^{WW} by isospin symmetry. Since isospin-breaking effects can be expected to be small, the uncertainty in this calculation is dominantly experimental. Together with $\Box^V_{\gamma Z}$ [7–14] and other one-loop corrections [1] this completes the one-loop analysis for the parity-violating part of the cross section.

To go beyond this result, one will need to perform challenging calculations of two-loop effects. The situation is expected to be particularly complicated when addressing nonperturbative contributions. It is not evident how a complete two-loop calculation at the hadronic level will be viable since it will involve the analysis of time-ordered products of three currents. While these hadronic effects are not enhanced by large electroweak logarithms, they may still be of importance at the $10^{-3} - 10^{-4}$ level which is the goal of the present analysis. Since it may not be possible to directly calculate these corrections, we aim at estimating the uncertainty which they may induce, together with the shift in the central value of Q_W^p.

Of particular interest is a subclass of two-loop hadronic corrections associated with the exchange of two bosons between the electron and proton, and another boson exchanged within the hadronic state. Since the loop integration is dominated by momenta of a typical hadronic scale, $\ell \lesssim \Lambda_h \sim 1$ GeV, one can conclude that the exchange of two heavy bosons, W or Z, will lead to corrections of $\mathcal{O}(\alpha G_F \Lambda_h^2)$ which are negligible. Furthermore, purely electromagnetic effects, i.e., diagrams with the exchange of photons only, cannot lead to a PV signature. Thus, only diagrams with at least one Z boson need to be considered. Among these, the only significantly new contribution arises from the exchange of two photons between the electron and the hadronic system, with parity violation within the latter. Such PV effects may arise due to mixing of hadronic states of equal spin and opposite parity. The parity-odd effect in 2γ exchange thus induces a parity-odd structure function $F_3^{\gamma\gamma}$ in the $\gamma\gamma$ box. Its effect should be added to $\Box^A_{\gamma Z}$ as it is indistinguishable experimentally.

In order to estimate this effect we use the picture in which gauge bosons mix with vector and axial-vector mesons. The photon mixes mostly with the vector mesons ρ, ω, and ϕ. Hadronic PV interactions can induce a_1-ρ mixing, effectively leading to a_1-γ mixing (left panel of Fig. 6). Similarly, PV state mixing in the isoscalar channel, such as h_1-ω, gives rise to h_1-γ mixing. But due to isovector dominance its numerical impact should be marginal (at the 10% level) and we disregard it. The Lagrangian describing the PV a_1-γ interaction can be written as

$$\mathcal{L}_{a_1\gamma} = \frac{e}{2} g_{a_1\gamma} F_{\mu\nu} a_1^{\mu\nu}, \tag{22}$$

where $F^{\mu\nu}$ and $a_1^{\mu\nu}$ are the field strength tensors of the photon and the a_1, respectively, and $g_{a_1\gamma}$ is the PV coupling constant.

To study the elastic component of $F_3^{\gamma\gamma}$, we first recall that (neglecting strangeness and the isoscalar axial coupling) the nucleon matrix element of the axial weak neutral current takes the form

$$\langle N|(J_Z^\mu)_A|N\rangle = g_A \bar{u}_N \gamma^\mu \gamma_5 \tau_3 u_N, \tag{23}$$

where $g_A = -1.27641(56)$ has been measured precisely in neutron beta decay [38,39]. The inclusion of the so-called nucleon anapole moment effectively shifts the apparent value of the nucleon axial charge seen in PV electron

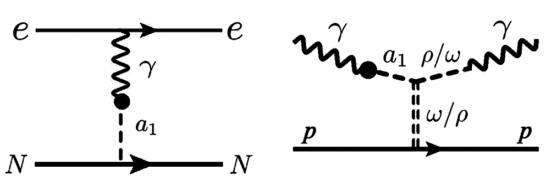

FIG. 6. Left: Effective description of the nucleon anapole moment. Right: Regge model description of PV in the forward $\gamma^* p$ Compton scattering amplitude.

scattering with respect to that in reactions involving charged current interactions, $g_A \to g_A + \delta g_A^{ep}$. Calculations based on hadronic parity violation in the framework of $SU(3)$ chiral perturbation theory [40] yield the result $\delta g_A^{ep} = 0.26(43)$ [41]. On the other hand, a global fit to PV electron scattering data not using theory constraints returns an even higher value: $\delta g_A^{ep} = 0.66(63)$ [42,43]. These results are consistent with each other, as well as with zero, but have large uncertainties impacting the error of the parity-violating asymmetry. In the picture where the anapole moment arises due to the effective a_1-γ mixing, as depicted in the left diagram of Fig. 6, the mixing strength $g_{a_1\gamma}$ is directly related to the value of δg_A^{ep}. The elastic contribution to $F_3^{\gamma\gamma}$ is then obtained as [44]

$$F_{3,\mathrm{el}}^{\gamma\gamma} = \frac{\delta g_A^{ep}}{g_A} F_{3,\mathrm{el}}^{\gamma Z} = -(0.20 \pm 0.34) F_{3,\mathrm{el}}^{\gamma Z}, \tag{24}$$

where the numerical estimate is based on the theory result [41].

Here we note an analogous relation for the correction to the Regge contribution discussed in the previous section:

$$F_{3,\mathbb{R}}^{\gamma\gamma} = \frac{\delta g_A^{ep}}{g_A} F_{3,\mathbb{R}}^{\gamma Z}, \tag{25}$$

which can be shown straightforwardly. This corresponds to a parity-odd effect which can be visualized by the right diagram of Fig. 6, where a photon mixes with an a_1 through Eq. (22) and then interacts with the nucleon through the exchange of a ρ/ω trajectory. Combining these two effects, we find an effective shift of $\Box_{\gamma Z}^A$ at P2 energies given by

$$\begin{aligned} \Box_{\gamma\gamma}^{PV} &= -(0.20 \pm 0.34)(\Box_{\gamma \mathrm{Z,el}}^A + \Box_{\gamma \mathrm{Z},\mathbb{R}}^A) \\ &= -2.3(3.8) \times 10^{-4}. \end{aligned} \tag{26}$$

One should keep in mind that further hadronic contributions not related to the anapole moment are possible, but their impact on the central value and the respective uncertainty is well below the target accuracy [44].

IV. SUMMARY AND CONCLUSIONS

We provided a thorough update of the $\Box_{\gamma Z}^A$ correction to PV electron-proton scattering. This calculation entails gathering all available information on the interference PV structure function $F_3^{\gamma Z}$ and its first Nachtmann moment over the full range of Q^2. The limiting cases of low and high Q^2 are governed by the elastic and DIS contributions, respectively. While these two contributions are known with good precision, the interpolation between them requires modeling inclusive hadronic contributions in the nonperturbative regime. This interpolation is the source of the uncertainty of the calculation. Luckily, the contributions from the intermediate Q^2 range are rather small, making the resulting model dependence not critical. In the past, the interpolation was performed by an essentially *ad hoc* procedure. In this work we invoke the isospin symmetry that is known to hold to a good extent and relate the neutral current interference structure function $F_3^{\gamma Z}$ to its charged current counterpart F_3^{WW} for which experimental data from inclusive neutrino and antineutrino scattering are available. Even though these data are not very precise, this procedure allowed us to better constrain the interpolation between the low- and high-Q^2 regimes, leading to a factor 2 reduction in the resulting uncertainty. In particular, for the P2 beam energy of $E = 155$ MeV we obtain from Table I

$$\Box_{\gamma Z}^A = (44.6 \pm 2.1) \times 10^{-4}, \tag{27}$$

which is in good agreement with Ref. [16] but with the uncertainty reduced by a factor of about 2. Including our result for $\gamma\gamma$ exchange with hadronic PV results in the total correction,

$$\Box_{\gamma Z}^A + \Box_{\gamma\gamma}^{PV} = (42.3 \pm 4.3) \times 10^{-4}. \tag{28}$$

This uncertainty is significantly larger than the one in Eq. (27). We note, however, that the P2 experiment [2] will in any case aim at reducing the uncertainty of the proton's anapole moment δg_A^{ep} by a factor of 4 via a dedicated backward angle measurement. The relevant uncertainty will then be the one in Eq. (27), while the small remaining one due to the induced PV photon-hadron interaction is 100% correlated with, and needs to be added linearly to, the tree-level g_A effect in the PV asymmetry.

Our calculation of the hadronic structure-dependent one-loop corrections due to the exchange of a γ and a Z boson between the electron and the proton has to be combined with other already known one-loop corrections [1,7–14]. This completes the one-loop analysis for the parity-violating part of the cross section.

Until a complete two-loop calculation is performed, one should try to identify the leading two-loop effects. We have done this for hadronic PV effects entering through $\gamma\gamma$ exchange. Our result shows that two-loop contributions to the PV asymmetry in electron proton scattering are numerically relevant. It seems less important now to work on further improvements of the one-loop results; instead, theoretical efforts should shift to the calculation of two-loop effects.

ACKNOWLEDGMENTS

This work was supported by the German-Mexican research collaboration Grant No. 278017 (CONACyT) and No. SP 778/4-1 (DFG). C.-Y. S. is supported in part by the DFG (Grant No. TRR110) and the NSFC (Grant

No. 11621131001) through the funds provided to the Sino-German CRC 110 "Symmetries and the Emergence of Structure in QCD" and also by the Alexander von Humboldt Foundation through a Humboldt Research Fellowship. M. G. acknowledges support by Helmholtz Institute Mainz. J. E. acknowledges support by PASPA (DGAPA-UNAM) and CONACyT Project No. 252167-F and is grateful for hospitality and support by the excellence cluster PRISMA$^+$ at JGU Mainz, as well as the Helmholtz-Institute Mainz.

[1] J. Erler and R. Ferro-Hernández, J. High Energy Phys. 03 (2018) 196.
[2] D. Becker *et al.*, Eur. Phys. J. A **54**, 208 (2018).
[3] J. Erler, A. Kurylov, and M. J. Ramsey-Musolf, Phys. Rev. D **68**, 016006 (2003).
[4] W. J. Marciano and A. Sirlin, Phys. Rev. D **27**, 552 (1983).
[5] W. J. Marciano and A. Sirlin, Phys. Rev. D **29**, 75 (1984); **31**, 213(E) (1985).
[6] D. Yu. Bardin, P. Christova, L. Kalinovskaya, and G. Passarino, Eur. Phys. J. C **22**, 99 (2001).
[7] M. Gorchtein and C. J. Horowitz, Phys. Rev. Lett. **102**, 091806 (2009).
[8] A. Sibirtsev, P. G. Blunden, W. Melnitchouk, and A. W. Thomas, Phys. Rev. D **82**, 013011 (2010).
[9] B. C. Rislow and C. E. Carlson, Phys. Rev. D **83**, 113007 (2011).
[10] M. Gorchtein, C. J. Horowitz, and M. J. Ramsey-Musolf, Phys. Rev. C **84**, 015502 (2011).
[11] N. L. Hall, P. G. Blunden, W. Melnitchouk, A. W. Thomas, and R. D. Young, Phys. Rev. D **88**, 013011 (2013).
[12] M. Gorchtein and X. Zhang, Phys. Lett. B **747**, 305 (2015).
[13] N. L. Hall, P. G. Blunden, W. Melnitchouk, A. W. Thomas, and R. D. Young, Phys. Lett. B **753**, 221 (2016).
[14] M. Gorchtein, H. Spiesberger, and X. Zhang, Phys. Lett. B **752**, 135 (2016).
[15] D. Androić *et al.* (Qweak Collaboration), Nature (London) **557**, 207 (2018).
[16] P. G. Blunden, W. Melnitchouk, and A. W. Thomas, Phys. Rev. Lett. **107**, 081801 (2011).
[17] P. G. Blunden, W. Melnitchouk, and A. W. Thomas, Phys. Rev. Lett. **109**, 262301 (2012).
[18] B. C. Rislow and C. E. Carlson, Phys. Rev. D **88**, 013018 (2013).
[19] C.-Y. Seng, M. Gorchtein, H. H. Patel, and M. J. Ramsey-Musolf, Phys. Rev. Lett. **121**, 241804 (2018).
[20] C. Y. Seng, M. Gorchtein, and M. J. Ramsey-Musolf, Phys. Rev. D **100**, 013001 (2019).
[21] J. Erler, Phys. Rev. D **59**, 054008 (1999).
[22] O. Nachtmann, Nucl. Phys. **B63**, 237 (1973).
[23] O. Nachtmann, Nucl. Phys. **B78**, 455 (1974).
[24] D. J. Gross and C. H. Llewellyn Smith, Nucl. Phys. **B14**, 337 (1969).
[25] A. L. Kataev and A. V. Sidorov, in *'94 QCD and high-energy hadronic interactions. Proceedings, Hadronic Session of the 29th Rencontres de Moriond, Moriond Particle Physics Meeting, Meribel les Allues, France, 1994* (Editions Frontieres, Gif-sur-Yvette Cedex, France, 1994), pp. 189–198.
[26] J. H. Kim *et al.*, Phys. Rev. Lett. **81**, 3595 (1998).
[27] C.-Y. Seng and U.-G. Meissner, Phys. Rev. Lett. **122**, 211802 (2019).
[28] Z. Ye, J. Arrington, R. J. Hill, and G. Lee, Phys. Lett. B **777**, 8 (2018).
[29] B. Bhattacharya, R. J. Hill, and G. Paz, Phys. Rev. D **84**, 073006 (2011).
[30] P. A. Baikov, K. G. Chetyrkin, and J. H. Kühn, Phys. Rev. Lett. **104**, 132004 (2010).
[31] P. A. Baikov, K. G. Chetyrkin, and J. H. Kühn, Nucl. Phys. B, Proc. Suppl. **205–206**, 237 (2010).
[32] J. D. Bjorken, Phys. Rev. **148**, 1467 (1966).
[33] K. G. Chetyrkin, J. H. Kühn, and M. Steinhauser, Comput. Phys. Commun. **133**, 43 (2000).
[34] O. Lalakulich and E. A. Paschos, Phys. Rev. D **71**, 074003 (2005).
[35] G. Onengut *et al.* (CHORUS Collaboration), Phys. Lett. B **632**, 65 (2006).
[36] T. Bolognese, P. Fritze, J. Morfin, D. H. Perkins, K. Powell, and W. G. Scott, Phys. Rev. Lett. **50**, 224 (1983).
[37] D. Allasia *et al.*, Z. Phys. C **28**, 321 (1985).
[38] B. Märkisch *et al.*, Phys. Rev. Lett. **122**, 242501 (2019).
[39] M. A. P. Brown *et al.* (UCNA Collaboration), Phys. Rev. C **97**, 035505 (2018).
[40] D. B. Kaplan and M. J. Savage, Nucl. Phys. **A556**, 653 (1993); **A580**, 679(E) (1994).
[41] S.-L. Zhu, S. J. Puglia, B. R. Holstein, and M. J. Ramsey-Musolf, Phys. Rev. D **62**, 033008 (2000).
[42] J. Liu, R. D. McKeown, and M. J. Ramsey-Musolf, Phys. Rev. C **76**, 025202 (2007).
[43] R. González-Jiménez, J. A. Caballero, and T. W. Donnelly, Phys. Rev. D **90**, 033002 (2014).
[44] M. Gorchtein and H. Spiesberger, Phys. Rev. C **94**, 055502 (2016).